

Scaling relationships between sizes of nucleation regions and eventual sizes of microearthquakes

メタデータ	言語: eng 出版者: 公開日: 2017-10-03 キーワード (Ja): キーワード (En): 作成者: メールアドレス: 所属:
URL	https://doi.org/10.24517/00010299

This work is licensed under a Creative Commons Attribution-NonCommercial-ShareAlike 3.0 International License.



Scaling relationships between sizes of nucleation regions and eventual sizes of microearthquakes

*Yoshihiro Hiramatsu and Muneyoshi Furumoto¹

Graduate School of Natural Science and Technology, Kanazawa University

Kakuma, Kanazawa, 920-1192, Japan

Phone: +81-76-264-6519

Fax: +81-76-264-6545

e-mail: yoshizo@hakusan.s.kanazawa-u.ac.jp; furumoto@hakusan.s.kanazawa-u.ac.jp

*corresponding author

1: now at Graduate School of Environmental Studies, Nagoya University

Furoo, Chikusa, Nagoya, 464-8601, Japan

e-mail: furumoto@eps.nagoya-u.ac.jp

Abstract

We investigate the initial rupture process of microearthquakes to reveal relationships between nucleation region sizes and eventual earthquake sizes. In order to obtain high quality waveform data, we installed a trigger recording system with a sampling frequency of 10 kHz at the base of a deep borehole at the Nojima Fault, Japan. We analyze waveform data of 31 events around the borehole, with seismic moment ranging from 4.2×10^9 Nm to 7.1×10^{11} Nm. We use both a circular crack model with an accelerating rupture velocity (SK model) (Sato and Kanamori, 1999), which generates a slow initial phase of velocity pulse, and a circular crack model with a constant rupture velocity (SH model) (Sato and Hirasawa, 1973), which generates a ramp-like velocity pulse. Source parameters of these two models are estimated by waveform inversion of the first half cycle of the observed velocity pulse applying both a grid search and a non-linear least squares method. 14 of 31 events are never reproduced by the SH model with a constant Q operator. But SK model with a constant Q operator provides a size of the pre-existing crack, corresponding to the size of the nucleation regions, and a size of

the eventual crack. We recognize that (i) the eventual seismic moment is approximately scaled as the cube of the size of pre-existing cracks, (ii) the eventual seismic moment is scaled as the cube of the size of eventual cracks, and (iii) the size of eventual cracks is roughly proportional to the size of pre-existing cracks. We, thus, conclude that the size of eventual earthquakes is controlled by the size of the nucleation regions.

Key words: initial rupture process, nucleation phase, nucleation region, scaling

Introduction

The initial rupture process is an important key to understanding the nucleation process of earthquake, because it may provide information of a nucleation region, if it exists. Some researchers reported that properties of the initial rupture process are causally related to the eventual size of an earthquake. The duration of a gradual increase of a velocity waveform of the initial part of the P-wave is called a slow initial phase (Iio, 1992; 1995) or a nucleation phase (Ellsworth and Beroza, 1995). This phase, as well as

the duration of the initial rupture (Umeda, 1990), scales with the eventual earthquake size. This kind of observation suggests that the existence of a nucleation region of an earthquake whose size might scale as the eventual size, as expected by rock experiments (e.g. Ohnaka and Kuwahara, 1990) and theoretical studies (e.g. Shibazaki and Matsu'ura, 1998). Shibazaki et al. (2002) reported that the slip velocity rose slowly with a low peak at the hypocenter area of the 1995 Hyogo-ken Nanbu earthquake (M7.2), supporting the existence of a nucleation region. However, Mori and Kanamori (1996) explained the observed weak initial phase using a circular fault model by Sato and Hirasawa (1973) (hereafter referred as the SH model) and constant Q operator. This means that the path effects apparently can cause a feature similar to a nucleation phase because SH model generates ramp-like onset of the velocity waveform in the far-field P-wave. On the other hand, another line of works rejected the path effects as the cause of nucleation phases. Deichmann (1997) concluded that a gradually accelerating rupture velocity could explain the observed waveform using a circular fault model with a gradually increasing rupture velocity (Sato, 1994). Iio et al. (1999) also reported that the observed slow initial phase was never generated by the path effects using the SH model.

The source model proposed by Sato and Kanamori (1999) (hereafter referred as the SK model) are useful for examining a relationship between the nucleation phase and the existence of a nucleation region, especially for microearthquakes. They assumed the existence of a circular pre-existing crack, corresponding to a nucleation region, and the radius of the pre-existing crack is an important factor to characterizing the shape of the waveform of the initial part of the P-wave. Applying the SK model with a constant Q operator, as well as applying the SH model, can clarify the cause of the nucleation phase, as a source effect, and the existence of a scaling relationship between the sizes of nucleation regions and the eventual sizes of earthquakes. Abiko et al. (1999) first applied the SK model to high quality waveform data in the western Nagano region, central Japan, with a sampling rate of 10 kHz. They confirmed that the nucleation phase was generated by the source process. Hiramatsu et al. (2002a) analyzed the initial rupture process of 12 microearthquakes recorded with 10kHz sampling at the base of a deep borehole at the Nojima fault using the SK model. They found that the nucleation phase of seven events was generated by the source process and the estimated sizes of nucleation regions seem to satisfy a scaling relationship derived by Ohnaka (2000).

More data should, however, be examined to confirm such a relationship.

In order to quantify properties of the initial rupture process of microearthquakes, we continue 10 kHz sampling observation of microearthquakes at the base of a deep borehole (1673m) at the Nojima Fault, similar to Hiramatsu et al. (2002a). In this paper, we analyze the initial rupture process of 31 events, which may be an adequate number of earthquakes to establish properties of the initial rupture process, ranging over two orders of seismic moment. We discuss scaling relationships of parameters, such as sizes of nucleation regions and eventual sizes of microearthquakes.

Data

The scientific program called the Nojima Fault-zone Probe drilled three boreholes with depths of 500, 800 and 1800 m into the fault zone at the southern end of the Nojima fault (Ando, 2001), which ruptured during the 1995 Hyogo-ken Nanbu earthquake. Velocity-type seismometers have been installed near the base of the 800 and 1800-m-deep boreholes (Ishii et al., 2001; Nishigami et al., 2001). In order to

investigate the fault zone properties and the healing process of the fault, water injection experiments at the Nojima fault were performed. The first injection was in 1997 (e.g. Tadokoro et al., 2000) and the second injection in 2000 (e.g. Nagai et al., 2001), with the operation of a temporary seismic network. After the second injection, local seismic observations have been continued to monitor seismicity around the borehole and the Nojima fault (Nagai et al., this issue). In order to study the source process of microearthquakes, it is necessary to observe those waveforms at close distance and minimize path effects, such as attenuation. Waveforms recorded at the base of deep boreholes can avoid the strong attenuation near the surface. We can expect to obtain good information about the sources from those data. All instruments are the same as reported by Hiramatsu et al. (2002a). All waveforms are recorded by a trigger recording system with a sampling frequency of 10 kHz (Iio et al., 1999) for the 1800-m-deep borehole, which provides high resolution of the initial part of P-waves. We observed more than 300 events around the borehole, whose source-receiver distances are 2~12 km, from June 2000 to December 2002. Rejecting poor quality data, we analyze waveform data of 31 events (Figure 1). The hypocenters of 19 of 31 events are reported

by the Japan Meteorological Agency (JMA) while others are determined in this study using records of the local seismic network. All the events analyzed in this study are not induced earthquakes by the water injection but also include background earthquake. Hiramatsu et al. (2002a) also analyzed background earthquakes except for one event. There is, thus, no essential difference of the data set between two studies. Seismic moments of these events are estimated by corner frequency analysis using an ω^{-2} model (Hiramatsu et al., 2002b) with a correction for the attenuation. We use the Q values and the source-receiver distance for the waveform inversion described below. Seismic moments range from 4.2×10^9 Nm to 7.4×10^{11} Nm. To minimize the noise, waveforms are averaged using a moving time window of 5 points (Iio, 1999). The typical ground noise level are reduced to $2 \times 10^{-7} \sim 3 \times 10^{-7}$ m/s. In the analysis, we use waveforms of the dominant component that shows the largest amplitude of the P-wave velocity pulse, recorded by the three component seismograph at the base (1673 m) of the 1800-m-deep borehole.

Source Models and Assumed Parameters

We apply two source models to the observed waveforms in this study. One model assumes a pre-existing crack and the rupture expands from the crack tip, and the other assumes the rupture initiates from a point. The former is a circular crack model with an accelerating rupture velocity proposed by Sato and Kanamori (1999)(the SK model), which generates a slow initial phase of the velocity pulse. The latter is a circular crack model with a constant rupture velocity by Sato and Hirasawa (1973)(the SH model), which generates a ramp-like velocity pulse. In calculating synthetic waveforms, we assume $V_p=5.5\text{km/s}$, $V_s=3.2\text{km/s}$, $\rho=2.7\text{g/cm}^3$, $\mu=32\text{GPa}$, and $\cos\phi=1$, where V_p is the P-wave velocity, V_s the S-wave velocity, ρ the density, μ the rigidity, and $\cos\phi$ the azimuthal term of the radiation pattern (Hiramatsu et al., 2002a). The parameters to be estimated for the SK model are δ (the trigger factor), l_0 (the half-length of the pre-existing crack), l_f (the half-length of the final crack), θ (the take off angle from fault normal), $\Delta\sigma$ (the stress drop), and Q (the quality factor). We choose values of 10^0 , 10^{-1} and 10^{-5} for δ and 50, 75, 100, 150 and 200 for Q to reduce the complexity of the calculations (Hiramatsu et al., 2002a). Parameters for the SH model are L (the

half-length of the final crack), θ , $\Delta\sigma$, and Q . We assume that the rupture velocity is 80% of the S wave velocity for the SH model. The source-receiver distance, R , is given by the S-P time measured by 10-kHz-sampling data and multiplying by 7.7 km/s, because the errors of the hypocenters determined by JMA and in this study not so small relative to the hypocentral distance. Synthetic waveforms are calculated by convolving the apparent moment rate function of each source model with the instrument response and the causal Q operator (Futtermann, 1962).

Waveform Inversion and Results

We estimate source parameters of these two models by waveform inversion of the first half cycle of the observed velocity pulse, using both a grid search and a non-linear least squares method (Hiramatsu et al., 2002a). Fitting the first half cycle of the pulse helps us to constrain a value of Q , because a lower Q value gives a broader pulse. The grid increments are 5° for θ , 1 m for L , l_0 , and l_f , 0.1 MPa for $\Delta\sigma$. Optimal source parameters are determined so that the $L2$ norm of the residual between the

observed and the synthetic waveforms becomes a minimum. The onset time of the P-wave is given by the time when the amplitude exceeds the noise level. We exclude waveforms that give unstable estimations of the source parameters for the perturbation of the noise level. The value of Q is an important factor in this study because some waveforms can be explained by various combinations of Q and δ . In this case, we adopt a Q value as low as possible to reject a possibility that the observed nucleation phase might be explained by the path effect. This procedure allows us to fit some waveforms, that can be explained by the combination of the SK model with $\delta=10^{-5}$ or $\delta=10^{-1}$ and higher Q , using the SH model, or using the SK model with $\delta=10^0$ and lower Q . We introduce a ratio of the $L2$ norm of the SK model to that of the SH model, $L2_{\text{SK}}/L2_{\text{SH}}$, as an indicator to judge which model is better. As shown in Figure 2, the difference of the pulse shape between the SH and SK models is subtle and is restricted only to the beginning part of the pulse. This means that there is a difficulty in using the whole shape of the pulse for distinguishing between the models. We, therefore, confirm the difference quantitatively using $L2_{\text{SK}}/L2_{\text{SH}}$ as given in Table 1. We emphasize again that the most important point is not the difference in the general shape of the pulse, but that

the gradual onset is never reproduced by the SH model. In general, it is difficult to distinguish a difference between waveforms reproduced by the SH model and those by the SK model with $\delta=10^0$ and $l_0\sim 1\text{m}$ (Hiramatsu et al., 2002a). In fact, in this case, the ratio of the $L2$ norms is around 1, indicating that the observed waveform is explained by both models. Some waveforms show large l_0 even in the case of $\delta=10^0$. However, we prefer not to use these values of l_0 in the following discussion because the value of $L2_{\text{SK}}/L2_{\text{SH}}$ are still close to 1. In this study, we judge that the SH model is insufficient to explain the observed waveform in cases that $L2_{\text{SK}}/L2_{\text{SH}}$ is less than 0.5. We use only data that satisfy this criterion for the following discussion on scaling relationships. As a result, 17 of 31 events can be explained both by the SH model and the SK model with $\delta=10^0$ (Figure 1 and Table 1). The remaining 14 events are reproduced well only by the SK model. As shown in Figure 2, the SH model fits the latter part from the peak of the pulse but fails to fit the beginning part of the pulse, which has a gradual increase of the velocity waveform. This result is independent of the choice of the values of the rupture velocity and Q . This means that the observed gradual increase is not a path effect but a source effect. In other words, this supports the existence of a nucleation region for

earthquakes. However, we have difficulty in determining uniquely source parameters of the SK model of these 14 events because the sizes of l_0 and l_f depend on the choice of δ . We have no criterion to judge which value of δ is appropriate because the resulted $L2$ norms are almost the same, independent of δ , 10^{-1} or 10^{-5} , and we recognize almost the same values for $L2_{SK}/L2_{SH}$. We regard the estimated l_0 and l_f for $\delta=10^{-5}$ as the lower limit and those for $\delta=10^{-1}$ as the upper limit (Hiramatsu et al., 2002a). All the estimated parameters are summarized in Table 1.

Scaling Relationships

Waveform inversions with the SK model of 14 events provides the set of the half-lengths of pre-existing cracks, l_0 , and the half-lengths of the eventual cracks, l_f . Based on these results, together with those of Hiramatsu et al. (2002a), it is worth examining the relationships among l_0 , l_f , and the eventual seismic moment, M_0 , as well as the duration of the nucleation phase reported previous works.

We show a relationship between l_0 and M_0 in Figure 3. In this figure we plot the

theoretical relationship, $M_0 = \alpha(2L_C)^3$ where $2L_C$ is a critical size of the nucleation region and α is a constant (Ohnaka, 2000). A pre-existing crack of the SK model can be interpreted as a quasi-static nucleation region (Sato and Kanamori, 1999). Ohnaka (2000) defined two critical sizes of a quasi-static nucleation zone $2L_{SC}$ and the initiation of high-speed rupture propagation $2L_C$. He formulated scaling relationships in terms of $2L_C$ to compare his model with seismological data. In his model, the dimension of L_{SC} is almost the same as that of L_C compared to the eventual source size. Thus, we assume $l_0 = L_C$ to apply his scaling relationship to our data. Our results satisfy well Ohnaka's relationship in a range between $\alpha = 10^6$ and $\alpha = 10^9$ for $\delta = 10^{-5}$ (Figure 3a) and for $\delta = 10^{-1}$ (Figure 3b). That is, the eventual seismic moment is scaled as l_0 , suggesting a causal relationship between the size of a nucleation region and the eventual size of an earthquake. In figure 4, we show a relationship between the radius of a nucleation region and the eventual seismic moment for a wide range of seismic moment from 10^9 Nm to 10^{22} Nm, using l_0 for $\delta = 10^{-5}$, together with the results of Beroza and Ellsworth (1996). Our results satisfy well the relation between the radius of a nucleation region and the eventual seismic moment reported by Beroza and Ellsworth (1996). We can also

recognize that Ohnaka's relationships hold well for the entire range of seismic moments. This indicates that there is a uniform scaling relationship, that is, the eventual seismic moment is scaled as the cube of the radius of the nucleation region over a range of seismic moments from 10^9 Nm to 10^{22} Nm.

Figure 5 shows a relationship between $\Delta\sigma$ for $\delta=10^{-5}$ and M_0 and the stress drop of a breakdown phase by Beroza and Ellsworth (1996). We assume that the estimated stress drop is equivalent to the dynamic stress drop of nucleation region (Sato and Kanamori, 1999). It is noteworthy that the breakdown stress drop is independent of the eventual seismic moment for a wide range of seismic moment. The estimated stress drop in this study may vary depending on values of the assumed parameters in the waveform inversion. However, such variations do not allow the breakdown stress drop to scale with the eventual seismic moment. Our results of scale-dependent l_0 can be interpreted as scale-dependent D_c , where D_c is the critical slip displacement, because the size of the nucleation region is proportional to D_c in the slip-dependent constitutive law (Ohnaka and Shen, 1999). This interpretation and scale-independent breakdown stress drop are consistent with conclusions of previous theoretical works (Shibazaki and

Matsu'ura, 1998; Ohnaka, 2000).

Figure 6 shows a relationship between l_f and M_0 . For reference, we draw lines of constant stress drop, $\Delta\sigma=(7/16)(M_0/r^3)$ where r is the radius of circular fault (Brune, 1970) under the assumption of $r=l_f$. We recognize that constant stress drop scaling holds well, that is the eventual seismic moment scales as the cube of l_f , both for $\delta=10^{-5}$ (Figure 6a) and for $\delta=10^{-1}$ (Figure 6b), using microearthquakes at the Nojima fault. In fact, the estimated stress drops from the waveform inversions lie in a typical range of $10^{-1}\sim 10^1$ MPa (Figure 5 and Table 1). This is consistent with the constant stress drop scaling law shown by corner frequency analyses using ω^{-2} models (Abercrombie, 1995; Hiramatsu et al., 2002b).

From the results shown in Figure 3 and Figure 6, we can expect a linear relationship between l_0 and l_f . Figure 7a shows a relationship between l_0 and l_f for $\delta=10^{-5}$. We recognize that l_f is roughly proportional to l_0 although the distribution of data has scatter. Our data lie in a range between $l_f=3l_0$ and $l_f=10l_0$ and is concentrating around $l_f=5l_0$. The same proportional relationship is recognized between l_0 and l_f for $\delta=10^{-1}$ (Figure 7b). The proportional coefficient is slightly smaller than that for $\delta=10^{-5}$ because

a smaller δ gives a larger l_0 . This figure shows that most data lie around $l_f=5l_0$, similar to the case for $\delta=10^{-5}$. We, thus, consider that a relationship $l_f\approx 5l_0$ might be typical for microearthquakes around the Nojima fault. An extrapolation of this scaling relationship to larger earthquakes seems to give a nucleation region which is larger than a size generally supposed. We stress that each microearthquake analyzed here is approximately a single crack. Large earthquakes usually consist of not a single asperity but several asperities. In these cases, an observable nucleation region may correspond to the size of the first asperity to break. We, thus, consider that the scaling relationship between l_0 and l_f estimated here gives the upper bound of the size of the nucleation region.

Finally, we mention the relevance of previous works focusing on the duration of the slow initial phase or the nucleation phase. Figure 8 shows a relationship between the duration of slow initial phases and the eventual seismic moments. We follow the definition of Iio (1992) to estimate the duration of a slow initial phase. We also plot the results reported by Iio (1995) and Beroza and Ellsworth (1996) in the same figure for comparison. Interestingly there seems to be a boundary between the durations for

waveforms explained only by the SK model with small δ and those explained both by the SH model and by the SK model with large δ . This boundary could be a threshold between waveforms with a nucleation phase from a source effect and those whose nucleation phase might be explained as a path effect, as shown in Iio (1999). Most of the results of the previous two studies lie above this threshold, indicating that a source process not a path effect generates the phases. Figure 9 shows a relationship between l_0 and the duration of the slow initial phase. It is natural that we recognize a proportional relationship between these quantities, as mentioned by Sato and Kanamori (1999). These figures show not only the validity of a simple definition of the duration of the nucleation phase by Iio (1992) but also a physical meaning of the slow initial phase. That is, a longer duration of the slow initial phase can be generated by a larger nucleation region, as shown in Beroza and Ellsworth (1996).

Conclusions

We analyze high quality waveform data with high sampling rate for 31

microearthquakes recorded at the base of a deep borehole at the Nojima fault, Japan. We apply source models proposed by Sato and Kanamori (1999) and Sato and Hirasawa (1973). The former assumes the existence of a pre-existing crack, resulting in a nucleation phase from the source. The latter assumes that a rupture initiates from a point, resulting in no nucleation phase. Applying these circular crack models with a constant Q operator, we confirm that nucleation phases of 14 events are generated not by a path effects but by a source process. From the estimated source parameters of the Sato and Kanamori model, together with those by Hiramatsu et al. (2002a), we recognize the following scaling relationships; (i) the eventual seismic moment is approximately scaled as the cube of the size of pre-existing cracks, (ii) the eventual seismic moment is scaled as the cube of the size of eventual cracks, and (iii) the size of eventual cracks is roughly proportional to the size of pre-existing cracks. We conclude that the size of the nucleation region controls the eventual size of microearthquakes.

Acknowledgements

We are grateful to Kin'ya Nishigami and Shiro Ohmi for their helpful assistance of recording and collecting the waveform data and Japan Meteorological Agency for providing the hypocentral catalogue. Comments of two anonymous reviewers and James J. Mori are useful to improve the manuscript. Generic Mapping Tools (Wessel and Smith, 1998) was used to draw some figures.

References

Abercrombie, R. E., 1995. Earthquake source scaling relationships from -1 to $5 M_L$ using seismograms recorded at 2.5-km depth, *J. Geophys. Res.*, 100, 24015-24036.

Abiko, Y., Sato, T., Iio, Y., 1999. Determination of source parameters for initial rupture process (2), Abstracts of SSJ Fall Meeting, P067.

Ando, M., 2001. Geological and geophysical studies of the Nojima fault from drilling: An outline of the Nojima Fault Zone Probe, *The Island Arc*, 10, 206-214.

Beroza, G. C., Ellsworth, W. L., 1996. Properties of the seismic nucleation phase, *Tectonophysics*, 261, 209-227.

Brune, J. N., 1970. Tectonic stress and the spectra of seismic shear waves from earthquake, *J. Geophys. Res.*, 75, 4997-5009.

Deichman, N., 1997. Far-field pulse shapes from circular sources with variable rupture velocities, *Bull. Seism. Soc. Am.*, 87, 1288-1296.

Ellsworth, W. L., Beroza, G. C., 1995. Seismic evidence for an earthquake nucleation phase, *Science*, 268, 851-855.

Futterman, W. I., 1962. Dispersive body waves, *J. Geophys. Res.*, 67, 5279-5291.

Hiramatsu, Y., Furumoto, M., Nishigami, K. Ohmi, S., 2002a. Initial rupture process of

microearthquakes recorded by high sampling borehole seismographs at the Nojima fault, central Japan, *Phys. Earth Planet. Int.*, 132, 269-279.

Hiramatsu, Y., Yamanaka, H., Tadokoro, K., Nishigami, K., Ohmi, S., 2002b. Scaling law between corner frequency and seismic moment of microearthquakes: Is the breakdown of the cube law a nature of earthquakes?, *Geophys. Res. Lett.*, 29 (8), 10.1029/2001GL013849.

Iio, Y., 1992. Slow initial phase of the P-wave velocity pulse generated by microearthquakes, *Geophys. Res. Lett.*, 19, 477-480.

Iio, Y., 1995. Observation of the slow initial phase generated by microearthquakes: Implications for earthquake nucleation and propagation, *J. Geophys. Res.*, 100, 15333-15349.

Iio, Y., Ohmi, S., Ikeda, R., Yamamoto, E., Ito, H., Sato, H., Kuwahara, Y., Ohminato,

T., Shibazaki, B., Ando, M., 1999. Slow initial phase generated by microearthquakes occurring in the Western Nagano prefecture, Japan –The source effect-, *Geophys. Res. Lett.*, 26, 1969-1972.

Ishii, H., Mukai, A., Fujimori, K., Nakao, S., Matsumoto S., Hirata, Y., 2001. Multi-component observation of crustal activity in the DPRI 800m borehole close to the Nojima Fault, *The Island Arc*, 282-287.

Mori, J., Kanamori, H., 1996. Initial rupture of earthquake in the 1995 Ridgecrest, California sequence, *Geophys. Res. Lett.*, 23, 2437-2440.

Nagai, S., Kano, Y., Tadokoro, K., Mizuno, T., Yamanaka, H., Ohmi, S., Nishigami, K., Hiramatsu, Y., Hirata, N., 2001. Microseismic observation during a water injection experiment in 2000 at the Nojima Fault, Japan (in Japanese with English abstract), *Bull. Earthq. Res. Inst.*, 76, 163-186.

Nagai, S., Tadokoro, K., Kano, Y., Yamamoto, K., Nishigami, K., Hirata, N., 2004. Analysis of similar events clusters around the Nojima fault water-injection site: Differences between injection-induced and natural seismicities, *Tectonophysics*, this issue.

Nishigami, K., Ando, M., Tadokoro, K., 2001. Seismic observation in the DPRI 1800m borehole drilled into the Nojima fault zone, southwest Japan, *The Island Arc*, 10: 288-295.

Ohnaka, M., 2000. A physical scaling relation between the size of an earthquake and its nucleation zone size, *Pure Appl. Geophys.*, 157, 2259-2282.

Ohnaka, M., Kuwahara, Y., 1990. Characteristic features of local breakdown near a crack-tip in the transition zone from nucleation to unstable rupture during stick-slip shear failure, *Tectonophysics*, 175, 197-220.

Ohnaka, M., Shen, L., 1999. Scaling of the shear rupture process from nucleation to dynamic propagation: Implications of geometric irregularity of the rupturing surfaces, *J. Geophys. Res.*, 104: 817-844.

Sato, T., 1994. Seismic radiation from circular cracks growing at variable rupture velocity, *Bull. Seism. soc. Am.*, 84, 1199-1215.

Sato, T, Hirasawa, T., 1973. Body wave spectra from propagating shear cracks, *J. Phys. Earth*, 21, 415-431.

Sato, T., Kanamori, H., 1999. Beginning of earthquakes modeled with the Griffith's fracture criterion, *Bull. Seism. Soc. Am.*, 89, 80-93.

Shibazaki, B., Matsu'ura, M., 1998. Transition process from nucleation to high-speed rupture propagation: scaling from stick-slip experiments to natural earthquakes, *Geophys. J. Int.*, 132, 14-30.

Shibazaki, B., Yoshida, Y., Nakamura, M., Nakamura, M., Katao, H., 2002. Rupture nucleations in the 1995 Hyogo-ken Nanbu earthquake and its large aftershocks, *Geophys. J. Int.*, 149, 572-588.

Tadokoro, K., Ando, M., Nishigami, K., 2000. Induced earthquakes accompanying the water injection experiment at the Nojima fault zone, Japan: Seismicity and its migration, *J. Geophys. Res.*, 105, 6089-6104.

Umeda, Y., 1990. High-amplitude seismic waves radiated from the bright spot of an earthquake, *Tectonophysics*, 17, 81-92.

Wessel, P., Smith, W. H. F., 1998. New improved version of the Generic Mapping Tools released, *EOS Trans. AGU*, 79, 579.

Figure captions

Fig. 1. The distribution of hypocenters (circles) and the location of the borehole station (cross) used in this study. Solid circles are events whose waveforms are reproduced by only the SK model and open ones by both SH and SK models. The sizes of circles are proportional to the moment magnitude, M_w . Gray lines are the Quaternary active faults.

Fig. 2. Examples of velocity waveforms reproduced well by the SK model with a $\delta=10^{-5}$ and a large l_0 . Misfits to the SH model indicate that the gradual increasing onset is a source effect. Black line shows the observed waveform. Broken and dotted lines show synthetic waveforms by the SK model and by the SH model estimated by waveform inversion, respectively. Gray rectangles on the upper waveform show the windows of the lower waveform.

Fig. 3. The relationship between the half-length of pre-existing crack, l_0 , and the eventual seismic moment, M_0 , for (a) $\delta=10^{-5}$ and (b) $\delta=10^{-1}$. Solid circles are results of

this study and open circles are those of Hiramatsu et al. (2002a). Broken lines are theoretical relations, $M_0 = \alpha(2l_0)^3$ of constant α between the size of nucleation region and the eventual seismic moment by Ohnaka (2000).

Fig4. The relationship between the radius of a nucleation region and the eventual seismic moment. We plot l_0 for $\delta = 10^{-5}$ as the radius of nucleation region. Solid circles are results of this study, open circles are from Hiramatsu et al. (2002a), and open squares are from Beroza and Ellsworth (1996). Broken lines are theoretical relations, $M_0 = \alpha(2l_0)^3$ of constant α between the size of nucleation region and the eventual seismic moment by Ohnaka (2000).

Fig. 5. The relationship between the breakdown stress drop, $\Delta\sigma$, and the eventual seismic moment. Solid circles are $\Delta\sigma$ for $\delta = 10^{-5}$, open circles are from Hiramatsu et al. (2002a), and open squares are from Beroza and Ellsworth (1996).

Fig. 6. The relationship between the half-length of the final crack, l_f , and the eventual

seismic moment, M_0 , for (a) $\delta=10^{-5}$ and (b) $\delta=10^{-1}$. Solid circles are results of this study and open circles are from Hiramatsu et al. (2002a). Broken lines are theoretical relations of constant stress drop, $\Delta\sigma=(7/16)(M_0/r^3)$, by Brune (1970). We assume here $r=l_f$.

Fig. 7. The relationship between the half-length of pre-existing crack, l_0 , and the half-length of final crack, l_f , for (a) $\delta=10^{-5}$ and (b) $\delta=10^{-1}$. Solid circles are results of this study and open circles are from Hiramatsu et al. (2002a). Broken lines show proportional relationships between l_0 and l_f .

Fig. 8. The relationship between the seismic moment and the duration of the slow initial phase. The duration of the slow initial phase (SIP) is measured by following the definition of Iio (1992). Solid circles are data whose waveforms are explained by only the SK model. Open circles are data whose waveforms are explained well by both the SH and SK models. Crosses and pluses are data reported by Iio (1995) and Beroza and Ellsworth (1996), respectively.

Fig. 9. The relationship between the half-length of pre-existing crack, l_0 , and the duration of the slow initial phase (SIP) for (a) $\delta=10^{-5}$ and (b) $\delta=10^{-1}$. Solid circles are results of this study and open circles are from Hiramatsu et al. (2002a).

Table caption

Table 1. The list of the estimated source parameters in this study. δ is the trigger factor, l_0 (m) the half-length of the pre-existing crack, l_f (m) the half-length of the eventual crack of the SK model, θ ($^\circ$) the take off angle from the fault normal, $\Delta\sigma$ (MPa) the stress drop, L (m) the half-length of the final crack of the SH model, $L2_{SK}/L2_{SH}$ the ratio of the $L2$ norm of the SK model to the $L2$ norm of the SH model, Q the quality factor, R (km) the source-receiver distance, and M_0 (Nm) the seismic moment.

event	SK model										SH model										
	$\delta=10^{-5}$					$\delta=10^{-1}$					$\delta=10^0$										
	l_0	l_f	$\Delta\sigma$	θ	$L2_{SK}/L2_{SH}$	l_0	l_f	$\Delta\sigma$	θ	$L2_{SK}/L2_{SH}$	l_0	l_f	$\Delta\sigma$	θ	$L2_{SK}/L2_{SH}$	L	$\Delta\sigma$	θ	Q	R	M_O
0103110317	12.0	84.6	1.79	18.5	0.13	14.3	86.9	1.80	18.3	0.15						70.9	2.79	12.2	200	12.1	7.7×10^{11}
0103142225											0.5	13.6	1.24	27.6	0.99	10.4	2.11	33.5	75	1.2	1.2×10^{10}
0104151109	4.9	30.8	5.98	24.9	0.07	6.3	31.3	6.46	26.3	0.04						27.3	9.34	12.1	200	9.0	2.1×10^{11}
0104202330	6.8	48.3	0.82	25.3	0.25	7.9	49.3	0.83	25.3	0.25						40.4	1.06	19.9	200	9.0	2.6×10^{11}
0104211732											2.5	25.7	1.14	11.9	0.72	19.0	1.64	14.9	200	6.2	2.5×10^{11}
0105041146											0.1	29.3	0.61	17.5	1.18	23.2	1.00	20.8	200	7.4	2.4×10^{10}
0105101154											0.4	26.9	0.59	18.0	1.30	20.8	0.93	23.7	150	5.4	2.6×10^{10}
0105260307											3.1	36.7	1.01	30.7	0.75	27.7	1.61	36.6	150	7.1	8.7×10^{10}
0109211517	3.9	22.7	0.37	24.1	0.30	4.9	23.0	0.40	25.1	0.29						18.6	0.45	19.4	100	2.0	1.0×10^{10}
0110262249											1.3	60.8	0.29	33.8	0.84	47.9	0.51	43.2	100	5.1	1.1×10^{11}
0110300419											0.1	15.3	0.78	39.1	1.05	12.1	1.50	51.9	100	2.4	1.1×10^{10}
0111011434	6.1	33.6	1.30	23.0	0.22	7.6	33.9	1.43	25.3	0.22						28.8	2.01	11.4	200	8.6	9.5×10^{10}
0112052231											1.4	45.8	1.22	28.4	1.01	35.6	2.02	36.1	100	6.1	4.1×10^{11}
0201290052											2.6	86.8	1.67	13.0	0.98	67.6	2.57	16.3	75	7.3	7.4×10^{11}
0203090613											0.4	20.0	0.21	27.1	0.96	15.5	0.36	34.4	150	2.5	6.5×10^9
0203230351	14.3	76.9	1.20	17.5	0.14	18.3	78.7	1.29	18.4	0.13						67.9	1.62	10.2	200	10.2	4.5×10^{11}
0205100405	8.0	37.7	0.51	24.8	0.26	9.6	38.8	0.54	25.2	0.27						32.9	0.65	12.9	200	6.2	4.5×10^{10}
0205190523	4.1	29.4	0.71	16.2	0.46	4.9	29.8	0.72	16.8	0.42						23.7	1.36	9.7	200	6.8	2.1×10^{10}
0205191622	7.7	30.7	1.79	21.6	0.33	10.0	31.6	2.06	22.7	0.34						27.8	5.04	3.9	200	6.8	4.3×10^{10}
0205240513											1.2	28.0	1.2	11.8	1.00	21.6	1.96	13.9	200	6.2	3.1×10^{10}
0208010119	11.8	32.3	2.05	12.6	0.10	14.9	35.1	2.68	10.0	0.10						33.0	2.36	2.7	200	7.5	5.1×10^{10}
0208230226											1.2	24.4	0.47	37.0	0.96	18.4	0.88	49.2	100	3.3	3.5×10^{10}
0208250311											0.4	17.1	0.33	30.0	0.94	13.2	0.58	38.4	100	1.7	8.3×10^9
0208300335											0.3	29.7	1.53	14.9	1.32	13.2	0.57	38.4	200	8.5	1.2×10^{11}
0209130245	3.6	30.6	2.20	32.6	0.18	4.3	31.0	2.25	32.8	0.20						25.1	3.49	20.6	200	6.0	1.1×10^{11}
0210140918	2.1	8.1	8.36	9.5	0.42	3.0	8.1	8.87	14.9	0.46						7.7	8.00	4.7	100	1.7	4.2×10^9
0210211216											2.4	28.0	7.51	8.5	1.06	20.9	15.1	7.5	100	6.2	1.7×10^{11}
0210241356											4.2	62.2	0.81	30.8	0.88	46.4	1.36	39.2	200	8.5	3.1×10^{11}
0210301647	11.1	50.3	0.50	26.8	0.34	13.8	52.2	0.53	27.6	0.33						44.8	0.48	17.9	200	7.0	7.2×10^{10}
0211110424	6.3	30.8	1.14	23.6	0.07	7.8	31.6	1.22	24.6	0.04						26.8	1.79	10.3	200	6.7	5.5×10^{10}
0211171207											1.1	76.1	0.93	5.9	1.26	59.9	3.20	3.2	150	6.9	1.6×10^{11}

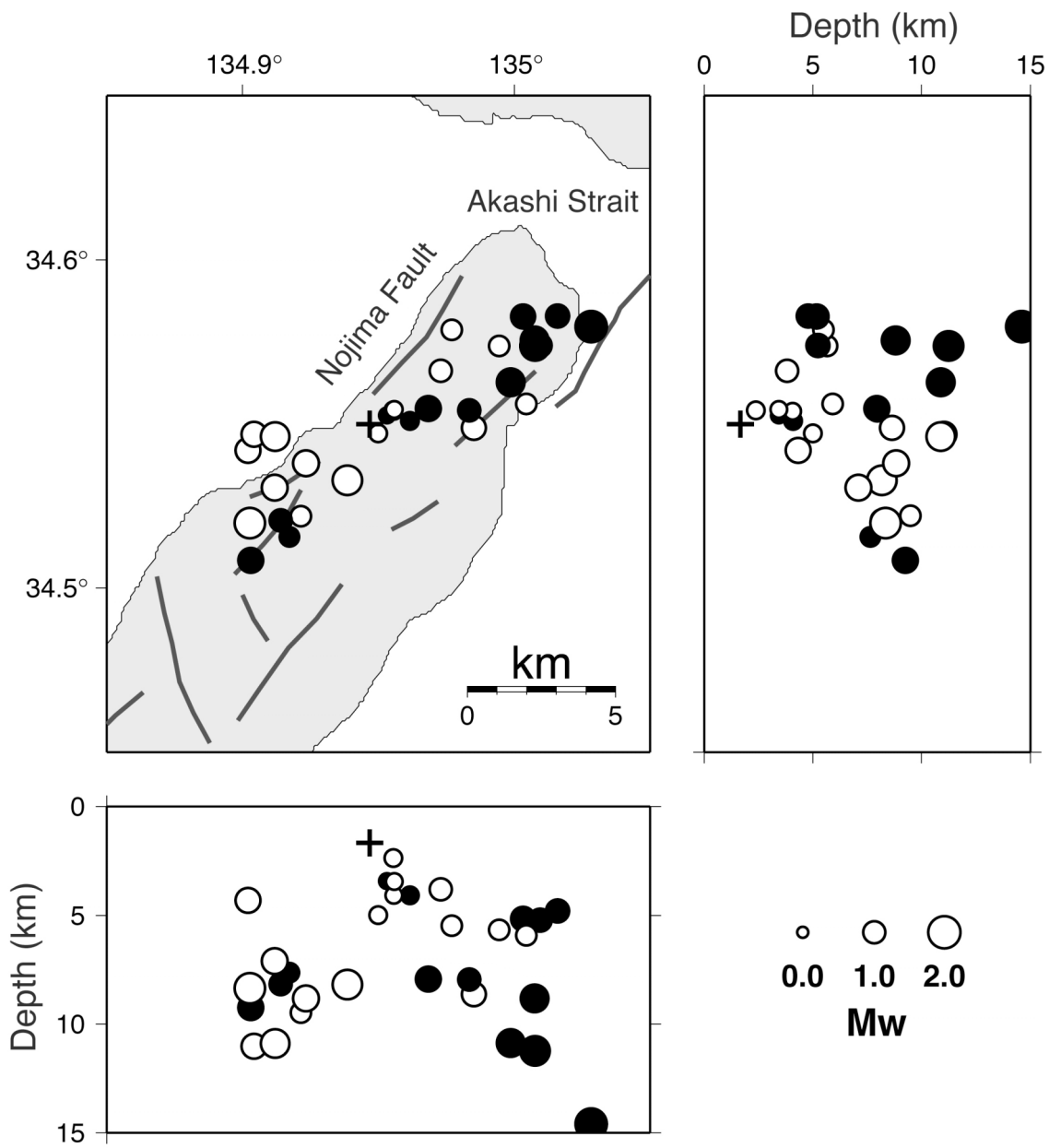


Figure 1. Hiramatsu and Furumoto

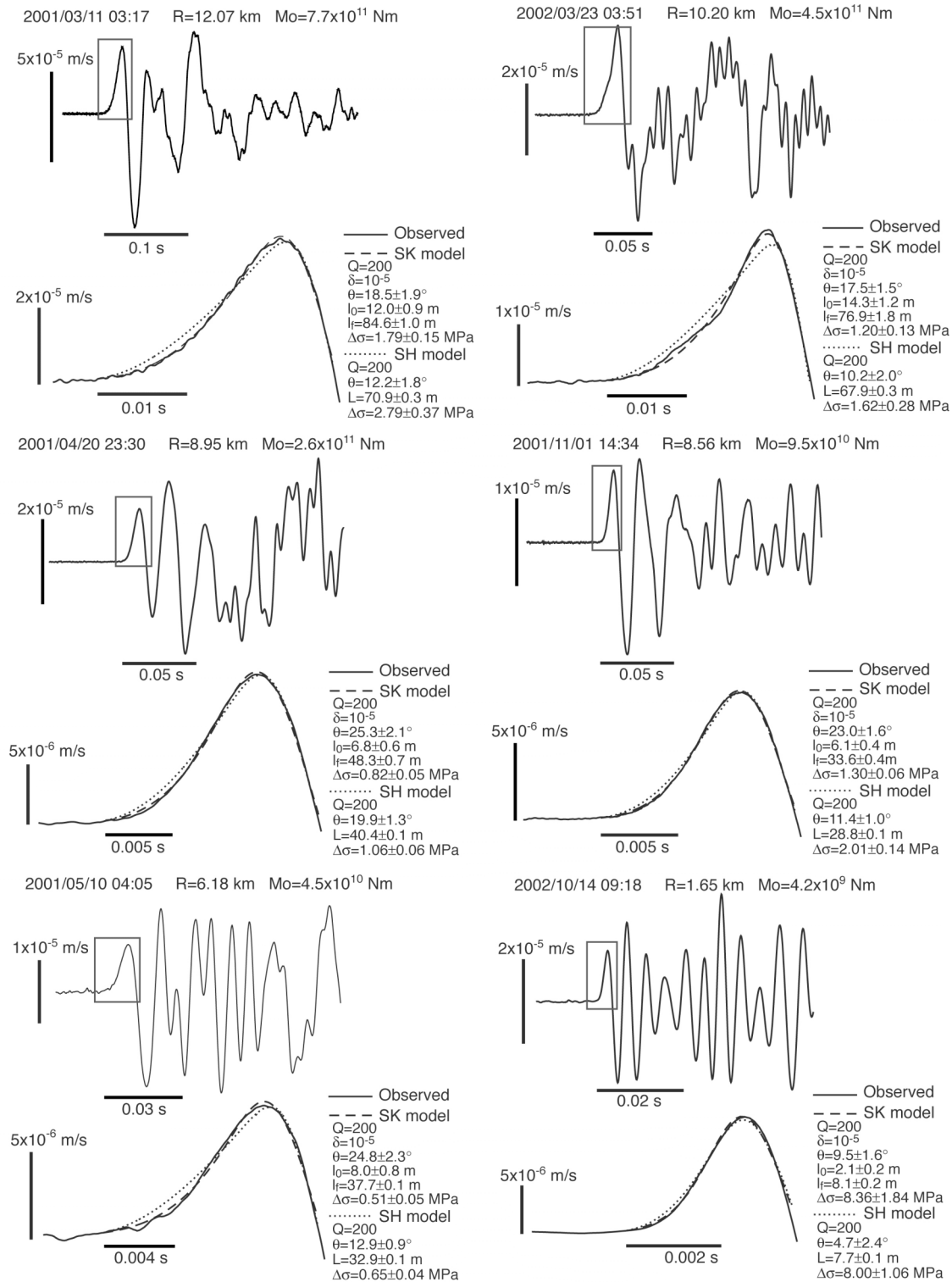


Figure 2. Hiramatsu and Furumoto

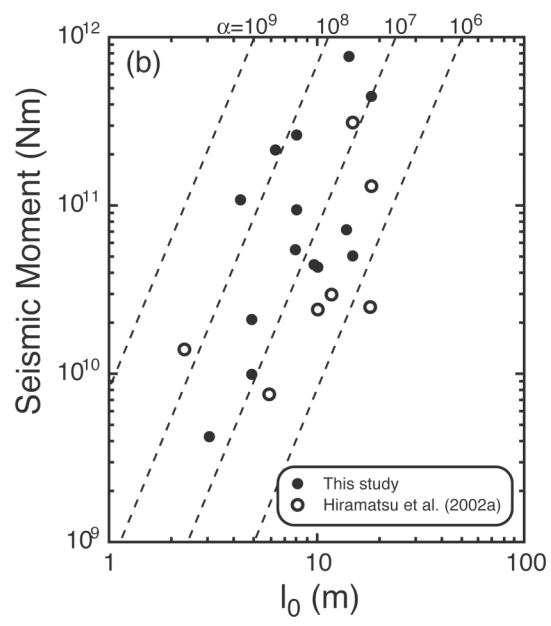
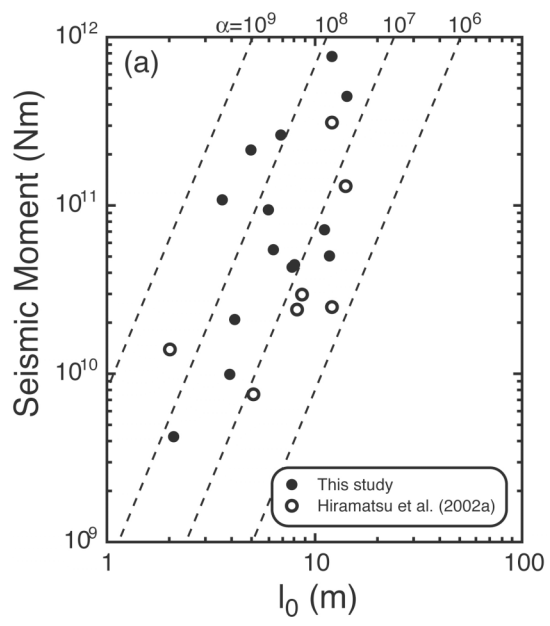


Figure 3. Hiramatsu and Furumoto

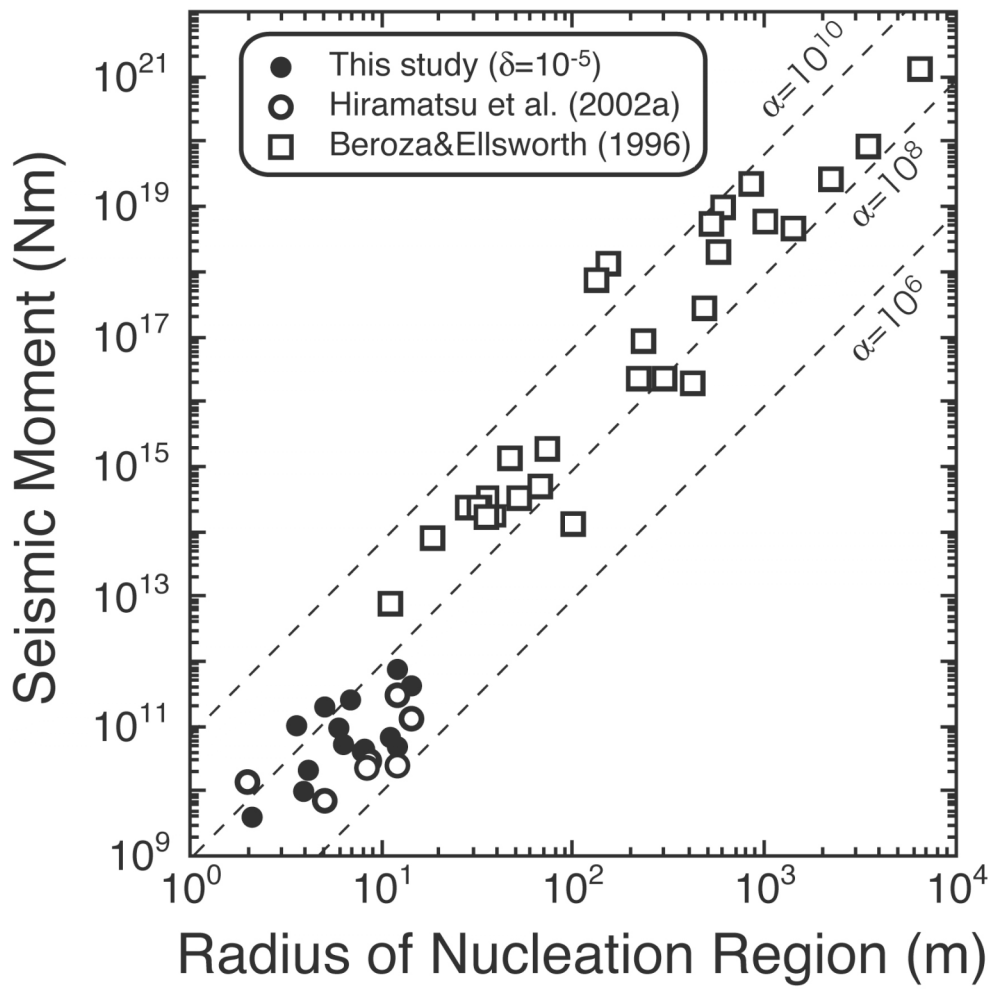


Figure 4. Hiramatsu and Furumoto

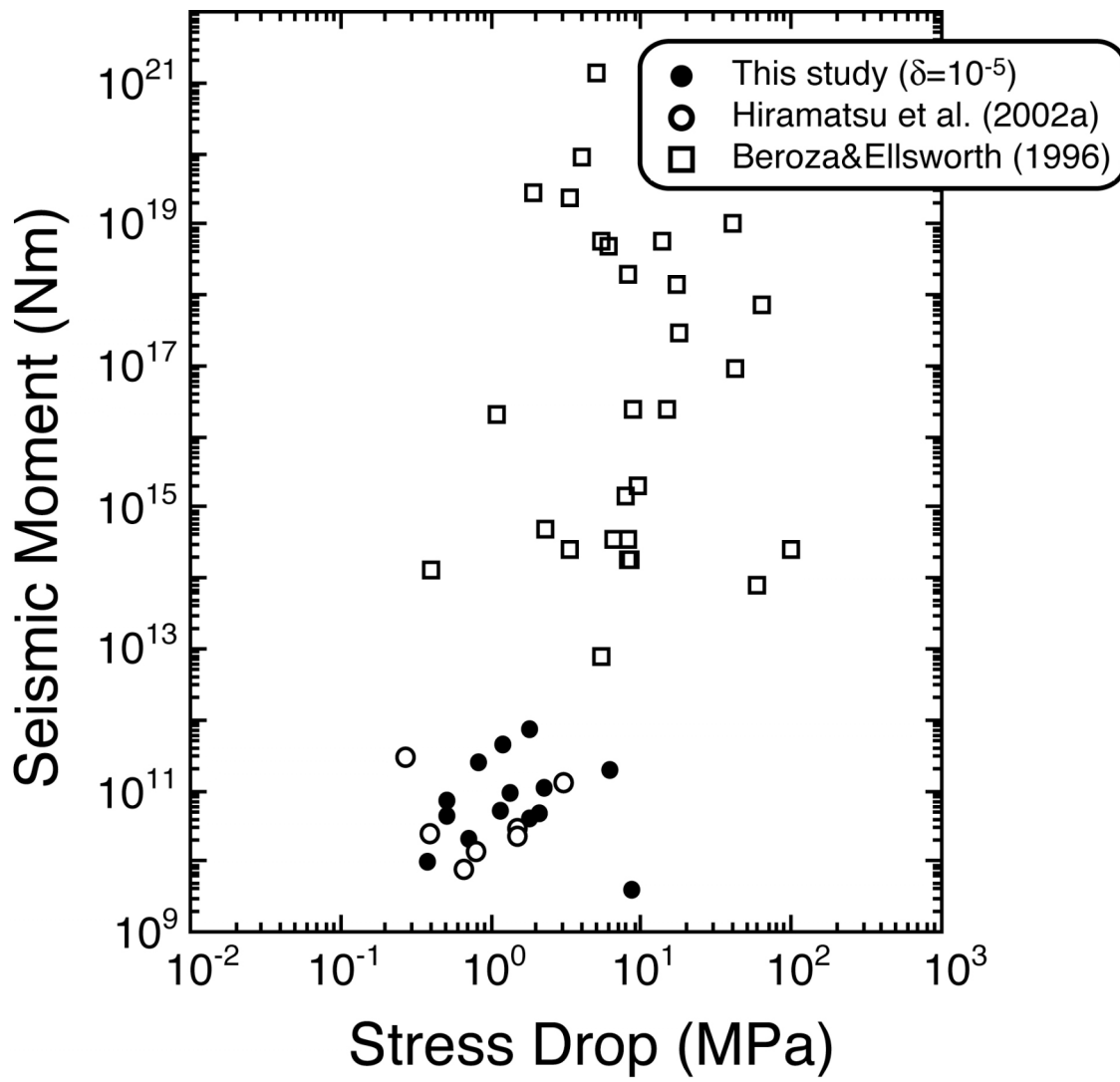


Figure 5. Hiramatsu and Furumoto

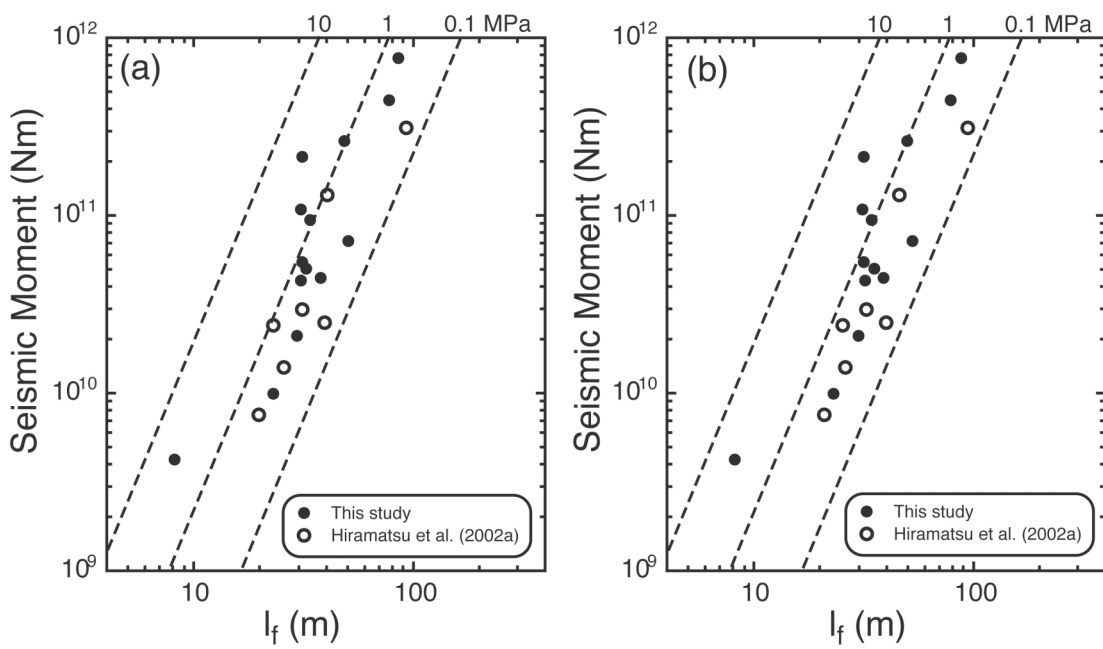


Figure 6. Hiramatsu and Furumoto

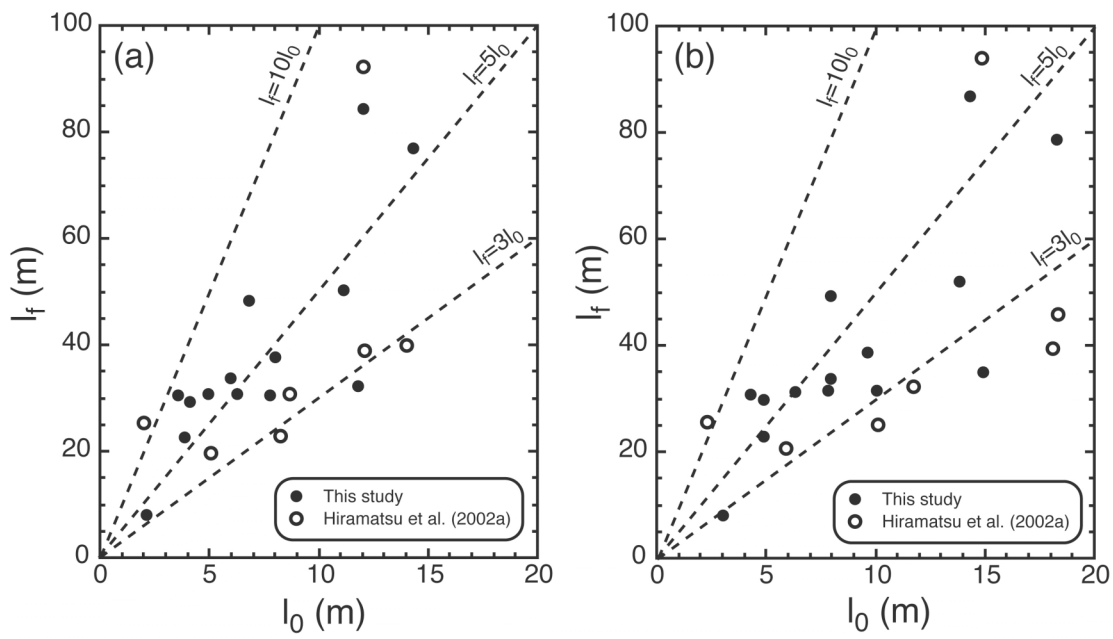


Figure 7. Hiramatsu and Furumoto

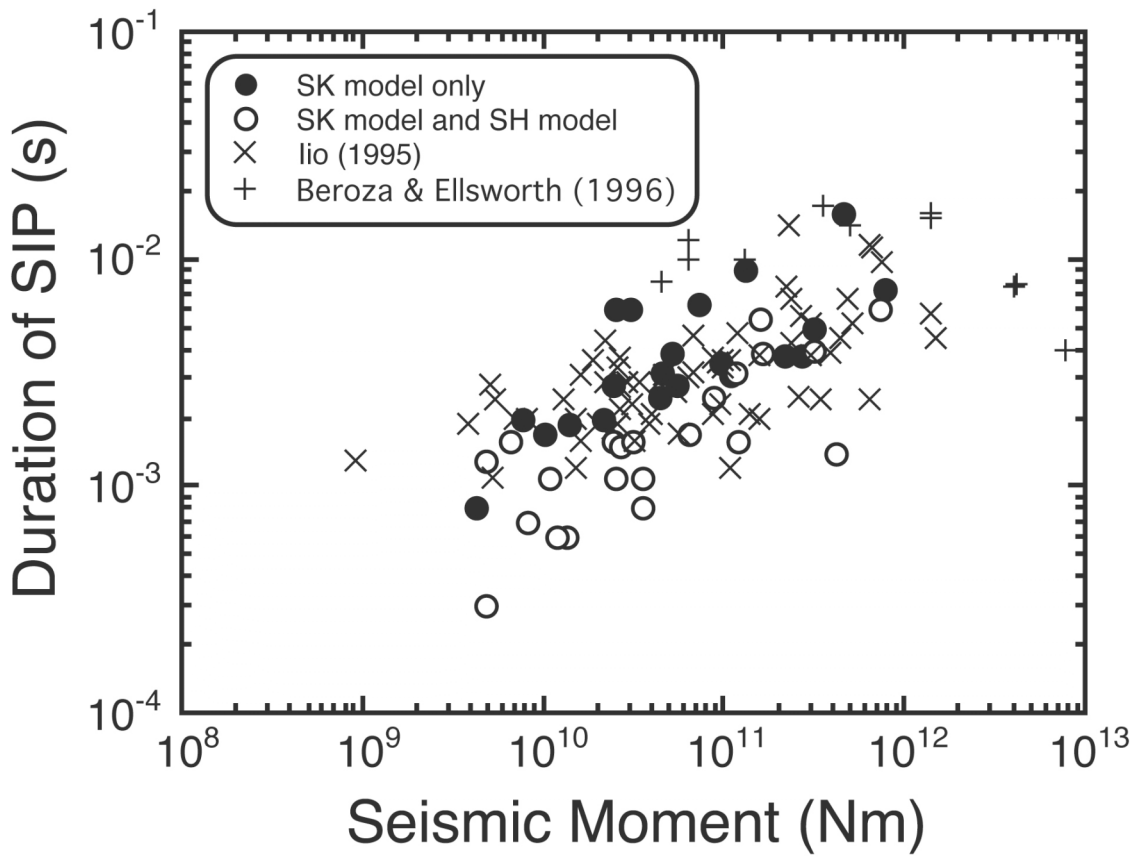


Figure 8. Hiramatsu and Furumoto

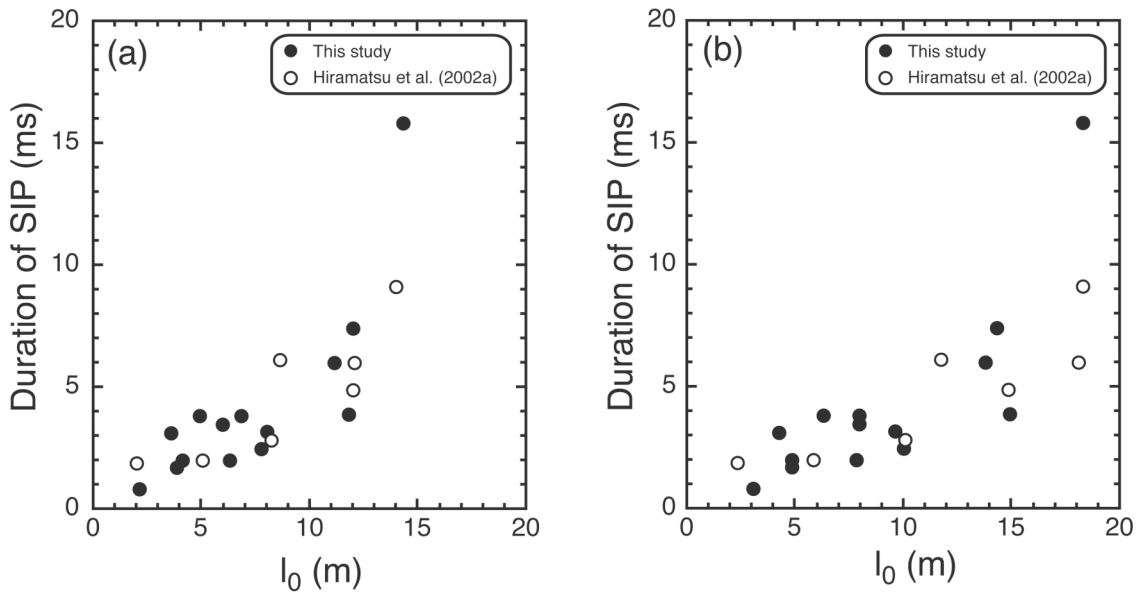


Figure 9. Hiramatsu and Furumoto

